Discharge rate balancing control strategy based on dynamic consensus algorithm for energy storage units in AC microgrids

Guan, Yajuan; Meng, Lexuan; Li, Chendan; Vasquez, Juan C.; Guerrero, Josep M.

Published in:
Proceedings of the 2017 IEEE Applied Power Electronics Conference and Exposition (APEC)

DOI (link to publication from Publisher):
10.1109/APEC.2017.7931093

Publication date:
2017

Document Version
Accepted author manuscript, peer reviewed version

Discharge Rate Balancing Control Strategy Based on Dynamic Consensus Algorithm for Energy Storage Units in AC Microgrids

Yajuan Guan, *Member, IEEE*, Lexuan Meng, *Member, IEEE*, Chendan Li, *Student Member, IEEE*, Juan C. Vasquez, *Senior Member, IEEE*, and Josep M. Guerrero, *Fellow, IEEE*
Department of Energy Technology, Aalborg University
Aalborg, Denmark
ygu@et.aau.dk, lme@et.aau.dk, che@et.aau.dk, juq@et.aau.dk, joz@et.aau.dk

***Abstract*— A dynamic consensus algorithm-based coordinated secondary control with an autonomous current-sharing control strategy is proposed in this paper for balancing discharge rate of energy storage systems (ESSs) in an islanded AC microgrid. The dynamic consensus algorithm is applied for information sharing between distributed generation (DG) units in order to regulate the output power of DGs according to ESS capacities and state-of-charge (SoC). The proposed controller can not only effectively prevent operation failure caused by over current and unintentional outage of DGs by means of balanced discharge rate control, but also provide fast response and accurate current sharing performance due to an autonomous current-sharing controller at primary level. In addition, expandability, flexibility and high reliability can be obtained thanks to the distributed architecture. Based on the developed linearized state-space model in z-domain, both the system stability and parameter sensitivity were analyzed. A comparison between experimental results obtained from using the conventional power sharing control and those obtained from the proposed coordinated control using a setup with three 2.2 kW DG units are presented to verify the effectiveness of the proposed controller.**

Keywords*— *Coordinated secondary control, dynamic consensus algorithm, energy storage units, balanced discharge rate, AC microgrids

I. INTRODUCTION

Microgrid is considered as a promising electric power system with decentralized power architecture, which supports a flexible electric grid by enabling the integration of renewable energy sources (RESs), energy storage systems (ESSs), and demand response [1], [2].

In view that a MG should be able to supply power to critical loads without the support of a utility grid and to overcome the intermittent nature of RESs, ESSs are needed in the case of grid-fault, energy-shortage, and load fluctuations. In this sense, it is advisable to equip more than one set of distributed ESS for providing redundancy so as to enhance both the system stability and reliability. Therefore, a coordinated control is required to guarantee stored energy balance among ESSs to avoid deep-discharge and over-charge.

The control capability of ESS is limited to its energy capacity. Meanwhile, the available electrical energy from ESSs is affected by various factors, such as charging conditions, ambient temperature, charging and discharging current, and aging [3]. Assuming the valve-regulated lead acid (VRLA) battery is considered as a power source for ESS in this case for its large number of charge-discharge cycles, deep discharge capability and low price. For one aspect, the depth of discharge (DOD) of a VRLA battery decreases exponentially with an increase in its lifecycle [4]. Hence, state-of-charge (SoC) usually has a limitation to prevent of deep-discharge. Another aspect is the capacity of a VRLA battery declines exponentially with an increase of discharge current [3]. Indeed, the total available electrical energy in VRLA batteries is variable in terms of discharge condition even though the batteries have the same initial SoC values. The conventional coordinated control strategies mainly focus on equal power sharing among DG units [1], [2]. However, the ESSs in different DG units can have different discharge rates according to their SoC and capacities. The powerless DG will first be shut down when its SoC is below the threshold, while the rest of DGs have to supply more power to the total loads. This situation may result in overcurrent and unintentional outages. Furthermore, it can degrade the stability and reliability of the MG.

To avoid this operation failure, all aspects of coordinated output power control strategy should be considered, such as the SoC and ESS capacities. In other words, the unit with the highest SoC should supply more power to the common load in order to ensure balanced discharge rate [5]. This kind of coordinated control strategy can be integrated to a hierarchical structure [6]. Several coordinated control strategies for SoC balancing in a MG have been proposed [7]-[14] in centralized or distributed topologies by means of combining communication technology with hierarchical control. In [9] an adaptive virtual resistance (VR) based droop controller is proposed to achieve stored energy balance. However, a centralized supervisory control is used which may result in a single point of failure.

The distributed control offers a more robust system and guarantees uninterruptible operation when either the network structure or electrical parameters are changed. On the other hand, consensus algorithms have been recently applied to MGs because of the effective way of sharing information among

DGs and facilitating the distributed coordination control [15], [16]. By using consensus algorithms, communication links are only needed between neighboring DG units, which can achieve plug 'n' play performance and reduce communication cost. A distributed multi-agent-based algorithm is proposed in [12] to achieve SoC balancing through voltage scheduling. A decentralized strategy based on fuzzy logic that ensures stored energy balance for a DC MG by modifying VRs of droop controllers is proposed in [13]. However, these control strategies were all developed in DC MG and based on droop control, which has a relatively slow transient response caused by low-pass filters [17]. Besides, both adaptive droop coefficients and variable voltage references seriously affect system stability in droop-controlled systems [18], [19].

Moreover, stability analysis for dynamic consensus-based MG, which includes both an electrical part in continuous-time domain and a consensus algorithm in discrete-time domain, is lack of sufficient study. Modeling in the discrete time domain is necessary to consider the discrete nature of communication. A modeling method in *z*-domain is proposed in [20].

In this paper, a novel coordinated secondary control for balanced discharge rate of ESS in an islanded AC MG is proposed. Instead of modified droop control, an autonomous current-sharing controller is employed at the primary level for AC MGs to achieve faster response and better accuracy in contrast to the control performance of droop control [21]. In addition, this control method provides large stability margin during parameters variations [18]. A dynamic consensus algorithm is implemented in each DG to share information for coordinately regulating the output power of DG units according to their SoC and ESS capacities by adjusting the VRs of the paralleled voltage-controlled inverters (VCIs). To analyze the system stability and parameter sensitivity, a detailed linearized discrete state-space model in *z*-domain including electrical part, primary control, and consensus algorithm is proposed.

II. Islanded Microgrid Configuration

A PV-ESS based islanded AC MG case-study scenario is shown in Fig. 1. The MG consists of several DG units, local loads, ESSs, power electronics interfaces and secondary control (SC) loop. Each DG unit includes a DC/DC converter and a three-phase DC/AC converter connected to AC bus, powered by PV panels and ESSs. With the dynamic consensus algorithm-based distributed secondary control, the SoC coordination control is implemented in each DG unit.

III. Proposed Balanced Discharge Rate Control

A. Primary control for current and power sharing

The used autonomous current-sharing control strategy in primary level is depicted in Fig. 2. The controller includes a synchronous-reference-frame phase-locked loop (SRF-PLL), a VR loop, and proportional resonant inner voltage and current controllers [21]. With this controller, a *d*-axis output current to angular frequency (I_{oq}–ω) and a *q*-axis output current to voltage magnitude (I_{od}–V) droop characteristics can be endowed in each inverter instead of adopting conventional power droop control in an AC MG. The relationships of

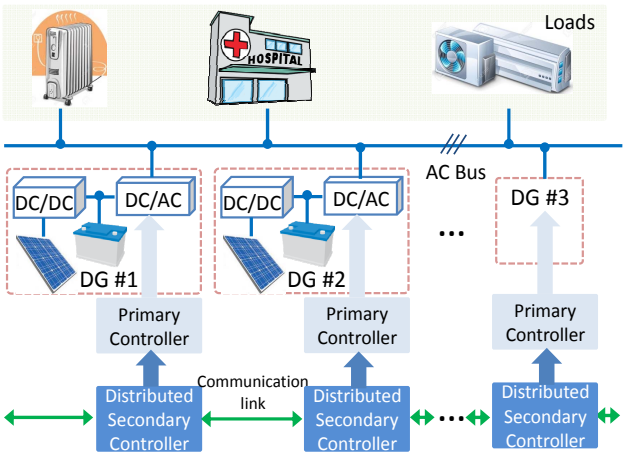

Fig. 1. A PV-ESS based MG case-study scenario.

I_{od}, I_{oq}, R_{virdn} and R_{virq} can be expressed for number N of converters as follows:

$$I_{od1}R_{virdn1} = I_{od2}R_{virdn2} = \cdots = I_{odN}R_{virdnN} \tag{1}$$

$$I_{oq1}R_{virq1} = I_{oq2}R_{virq2} = \cdots = I_{oqN}R_{virqN} \tag{2}$$

where R_{virdn} and R_{virqn} are the *d* and *q*-axis VRs of VCI #n.

Hence, the *d*- and *q*-axis output currents can be regulated independently by adjusting the VRs based on different power rates or commands from higher level controllers. Additionally, the active and reactive power output sharing among the paralleled VCIs can be achieved from (1) and (2) by multiplying the voltage reference. The active and reactive power outputs can be properly shared based on VR ratios as well, as shown below:

$$P_{o1}R_{virdn1} = P_{o2}R_{virdn2} = \ldots = P_{oN}R_{virdnN} \tag{3}$$

$$Q_{o1}R_{virq1} = Q_{o2}R_{virq2} = \ldots = Q_{oN}R_{virqN} \tag{4}$$

where P_{on} and Q_{on} are the active and reactive power outputs of VCI #*n*.

B. SoC estimation and discharge rate calculation

The energy consumption of ESS_i can be represented by the integration of the output active power of DG #*i* (P_i) [22]. Therefore, the SoC of ESS_i can be calculated as follows:

$$SoC_i = 1 - \frac{k}{C_{bat\_i}} \int P_i \mathrm{d}t \tag{5}$$

where k is a change ratio for time scale and is equal to 1/3600; C_{bat_i} is the rated capacity of ESS_i; P_i is the output active power

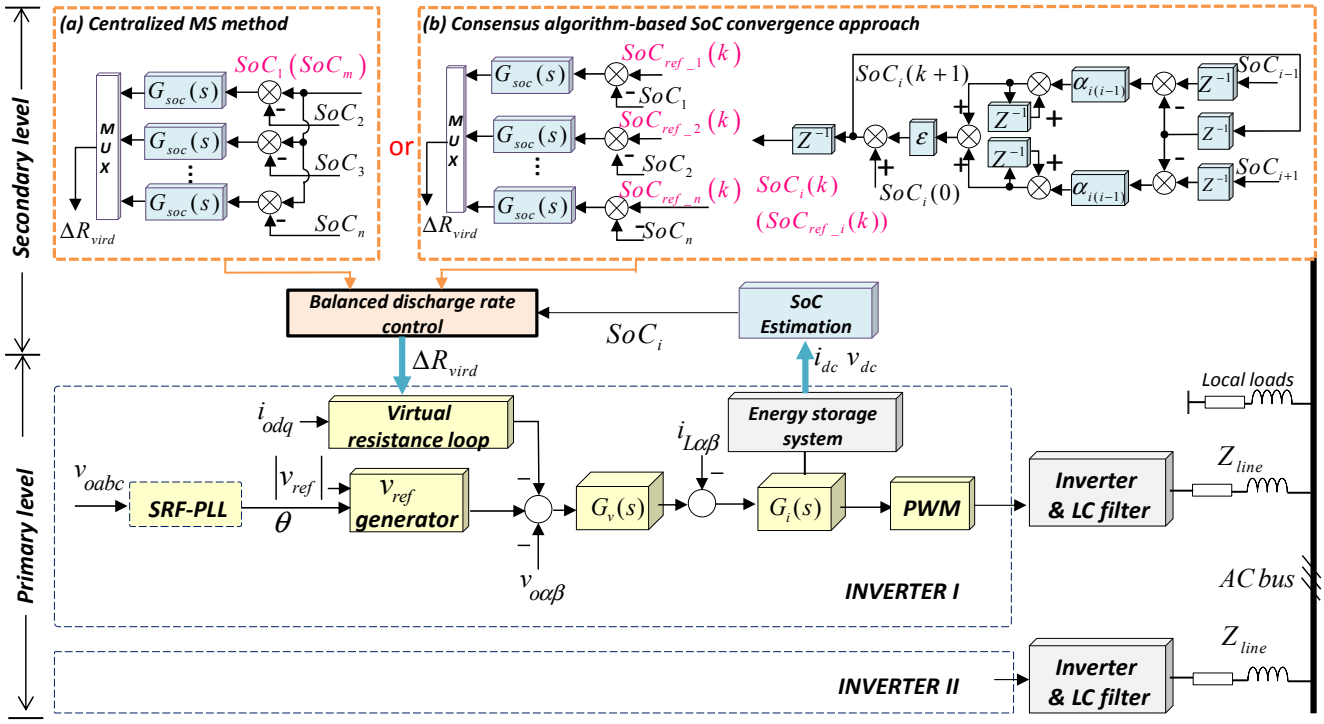

Fig. 2. Proposed dynamic consensus algorithm-based SoC coordinated control strategy.

of DG #*i*.

The discharge rate of DG #*i* (η_i) can be defined as follows:

$$\eta_i = \frac{d}{dt} SoC_i = -\frac{k}{C_{bat\_i}} P_i \tag{6}$$

The definition shows that the discharge rate is influenced by the rated capacities of ESSs and the output active power of DG #*i*. Thus, the coordinated control and equal discharge rate can be obtained by regulating each VR based on their respective SoC and ESS capacities because the load sharing ratio among DG units is dominated by VR ratio.

C. Information sharing with dynamic consensus algorithm

With regard to MGs, a consensus algorithm can be used to eliminate the dependence on a signal DG, achieve the information sharing and coordination among DG units and to reduce communication cost. In this technique, each DG unit only communicates its state to adjacent DGs. Every DG in the network updates its state by providing a linear equation of its own state and neighbors' states. Finally, the states of all DGs are able to reach a convergence of the desired average value. A connected MG system can be presented by a graph, $G_{MG} = (N_n, E)$, which is composed of a set of nodes, N_n, and a set of edges, E. In this case, a node represents a DG unit. If i and j denote two different nodes, the edge, $\{i,j\} \in E$, presents a bidirectional communication link.

To maintain the accurate convergence in dynamically changing networks while simultaneously handling the discrete communication data exchange, a dynamic consensus algorithm is applied as follows [16]:

$$x_i(k+1) = z_i + \varepsilon \sum_{j \in N_i} \delta_{ij}(k+1) \tag{7}$$

$$\delta_{ij}(k+1) = \delta_{ij}(k) + \alpha_{ij}\left(x_j(k) - x_i(k)\right) \tag{8}$$

where x_i and x_j are the states stored in nodes i and j; $i, j = 1, 2, \ldots, N$, $\{i, j\} \in E$; α_{ij} presents the connection status between nodes i and j; ε is the constant edge weight. z_i is the initial state of node i, and $\delta_{ij}(0)$ is equal to zero. In this sense, each node updates its state based on the stored value, connection scheme, scalar tuning parameters, and stored values of all the neighboring nodes. Besides, with (7), the final convergence value is related to the initial state, z_i, which means that regardless of the degree of change that occurs in z_i, the algorithm can converge to the desired average value.

Regarding the real physical meaning, the output variables, $x_i(k+1)$, $i, j = 1, 2, \ldots, N$, and $\{i, j\} \in E$, become the SoC references, SoC_{ref_i}, for each DG unit in this paper. Thus, (7) and (8) can be rewritten as follows:

$$SoC_{ref\_i}(k+1) = SoC_i(0) + \varepsilon \sum_{j \in N_i} \delta_{ij}(k+1) \tag{9}$$

$$\delta_{ij}(k+1) = \delta_{ij}(k) + \alpha_{ij}\left(SoC_j(k) - SoC_i(k)\right) \tag{10}$$

The edge weight, ε, can be taken as a turning parameter to minimize the convergence time for a given communication network when it meets the following equation [23]:

$$\varepsilon = \frac{2}{\lambda_{\max}(\boldsymbol{L}) + \lambda_{n-1}(\boldsymbol{L})} \tag{11}$$

where $\boldsymbol{L}$ is the Laplacian matrix of graph G_{MG} [24], $\lambda_{max}(\boldsymbol{L})$ represents the largest eigenvalue of $\boldsymbol{L}$, while $\lambda_{n-1}(\boldsymbol{L})$ denotes the second smallest eigenvalue of the Laplacian matrix. In this case, ε=1/3 is the optimized weight parameter.

D. Proposed coordinated secondary control for balanced discharge rate

The centralized master-slaver (MS) SoC coordinated control is show in Fig. 2(a). By contrast, the complete control scheme of the proposed distributed dynamic consensus algorithm-based SoC coordinated secondary control strategy is shown in Fig. 2(b). At the secondary control level, dynamic consensus algorithm is implemented for enabling a set of DG units to agree on a control variable by exchanging information through communication networks. In this case, it takes charge of finding the averaged value of SoC for each DG by means of the outputs of SoC estimation loops and the network configuration. Hypothetically, each ESS is fully charged at the beginning, which means that each initial SoC is equal to 1. The idea is to balance the discharge rate of each DG unit according to its ESS capacities to avoid overcurrent and unintentional outage. The differences between the measured SoC_i and the desired average SoC_{ref_i} obtained from dynamic consensus algorithm are sent to PI controllers which outputs are taken as increments in *d*-axis VR to adjust the output currents of DG units. The increments of *d*-axis VR can be expressed as follow:

$$\Delta R_{vird\_i} = K_p(SoC_{ref\_i} - SoC_i) + K_i\int(SoC_{ref\_i} - SoC_i)dt \tag{12}$$

where K_p and K_i are the parameters of the PI controllers. To reduce the power oscillation, the outputs of PI controllers are regarded as incremental control parts. Therefore, the updated *d*-axis VR of each DG can be presented as follow:

$$R_{vird\_i} = R_{vird\_b} + \Delta R_{vird\_i} \qquad i = 1,2,3,4.....N \tag{13}$$

where R_{vird_i} is the *d*-axis VR for DG #*i*; R_{vird_b} is the basic *d*-axis VR; in this case, R_{vird_b} is preassigned to 4 Ω [21]; ΔR_{vird_i} is the increment output from the PI controller.

Therefore, the adaptive *d*-axis VRs can be considered as turning parameters to adjust the direct current outputs and active power outputs of parallel-connected DG units with respect to their SoC values and different ESS capacities.

IV. Linearized State Space Model and Stability Analysis

To analyze the system stability and parameter sensitivity, the developed state-space model of the proposed coordinated secondary controller is discussed based on a three-paralleled-DG system. The state-space model is mainly divided into two parts: sub-models of SoC controller and MG plant in the continuous time domain and sub-model of consensus algorithm in the discrete time domain.

A. Linearized discrete model

In order to integrate overall state-space model, the combination of SoC controller and MG plant model needs to be discretized to equivalent discrete time model with sampling time T_{con} which is applied for communication.

As the inputs of SoC consensus algorithm loop are the initial SoC states of DG units, while the outputs are the states obtained for each DG unit at *k*th iteration, $SoC_{ref\_i}(k)$. Based on (9) and (10), two state variables exist in the dynamic consensus algorithm control loop. One of the state variables is the internal cumulative difference between node *i* and *j*, $\delta_{ij}(k)$, $j \in N_i$ which is the set of neighbors of node *i*. The other is the output state $x_i(k)$, which has a practical physical meaning of $SoC_{ref\_i}(k)$.

A complete linearized discrete state-space model of the proposed three-DG-unit system can be obtained by combining the following sub-state-space models: the combined SoC controller and MG plant model in discrete time domain and the dynamic consensus algorithm model. A total of 18 states are included:

$$X^{dis}(k+1) = G^{dis}X^{dis}(k) + H^{dis}u^{dis} \tag{14}$$

being

$$X^{dis} = [X_{1\_1}\ X_{1\_2}\ X_{1\_3}\ X_{2\_1}\ X_{2\_2}\ X_{2\_3}\ X_{3\_1}\ X_{3\_2}\ X_{3\_3}\ \delta_{12}\ \delta_{13}\ \delta_{21}\ \delta_{22}\ \delta_{31}\ \delta_{32}\ SoC_{ref\_1}\ SoC_{ref\_2}\ SoC_{ref\_3}]^T$$

where X_{1_i}, X_{2_i}, and X_{3_i} (*i*=1, 2, and 3) present the state variables of the discrete sub-models of SoC controller and MG plant model for DG #*i*.

B. Stability analysis based on linearized discrete model

To analyze system stability and adjust the parameters to obtain the desired transient response of the proposed system, *z*-domain root locus plots of (14) are represented as a function of different parameter variations. The system parameters and equilibrium point are listed in Table I.

Fig. 3 shows the root locus in the discrete-time domain for the system as a function of the variation of the proportional term in SoC regulator K_p from 0.1 to 1000. The system has an underdamped response for higher values of K_p. The system could maintain stability as the eigenvalues are displaced within the unit circle.

Fig. 4 shows the root locus plot for the system that corresponds to a variation of the integral term, K_i, in the range of 1 to 10000. The figure shows that an increase in K_i leads to two pairs of complex conjugated poles λ_6, λ_7, λ_8, and λ_9, which results in oscillation. However, K_i has a small effect on the movements of dominating poles.

As illustrated in Figs. 4 and 5, the paralleled DG system with the proposed controller presents low sensitivity of the parameters at secondary level over the system dynamics due to the large stability margin provided by the employed autonomous current sharing control at primary level [19]. Hence, the proposed control approach can achieve more stable

TABLE I
MODEL PARAMETERS AND EQUILIBRIUM POINT

Model Parameters					
Symbol	**value**	**Symbol**	**value**	**Symbol**	**value**
$C_{bat\_1/2/3}$	10/20/30 Wh	K_p	12	K_i	1000
$R_{vird\_b1/2/3}$	4/4/4 Ω	k	1/3600		
Equilibrium Point					
Symbol	**value**	**Symbol**	**value**	**Symbol**	**value**
$R_{\text{vird}\_1}^{equ}$	6.042	P_1^{equ}	197.4 W	$SoC_{ref\_1}(0)$	1
$R_{\text{vird}\_2}^{equ}$	2.896	P_2^{equ}	401.4 W	$SoC_{ref\_2}(0)$	1
$R_{\text{vird}\_3}^{equ}$	1.953	P_3^{equ}	590.3 W	$SoC_{ref\_3}(0)$	1

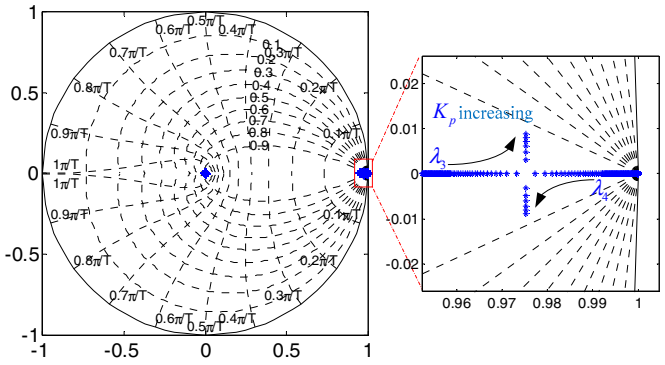

Fig. 3. Trace of modes as a function of proportional term of SoC regulator: $0.1 < K_p < 1000$.

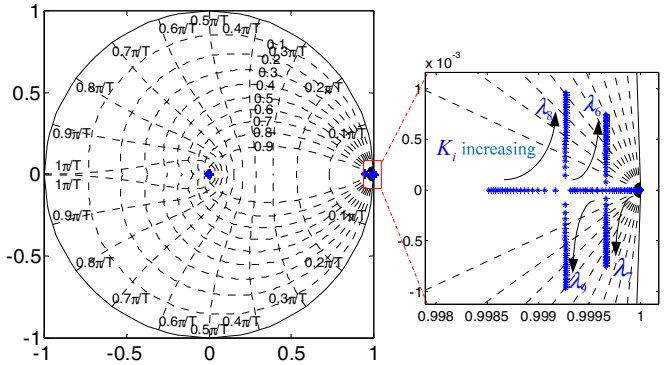

Fig. 4. Trace of modes as a function of integral term of SoC regulator: $1 < K_i < 10000$.

control performance compared with droop-based SoC coordinated controller.

V. EXPERIMENTAL RESULTS

An islanded experimental MG setup consisted of three three-phase inverters formed as a three-DG-unit system has been built, as shown in Fig. 5. The Danfoss inverters were used to simulate different DG units with different ESS capacities. Different case-study scenarios were considered for verifying the control performance of the proposed dynamic consensus algorithm-based coordinated control strategy. Before the experiments were conducted, the required assumptions were met. First, ESS_i in each DG unit was fully charged. Thus, each $SoC_{ref\_i}(0)$ was equal to 1. Second, the minimum threshold of SoC was set at 0.3. Third, the ESS capacities of the three DG units were different. C_{bat_1}, C_{bat_2}, and C_{bat_3} were equal to 10,

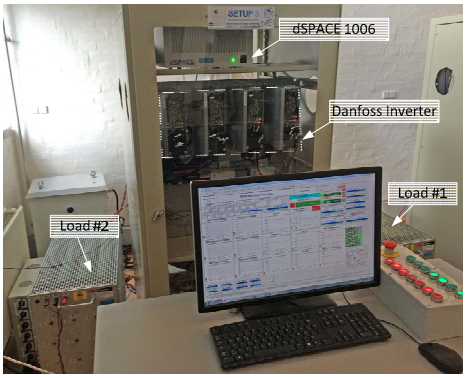

Fig. 5. Experimental setup.

TABLE II
POWER STAGE AND CONTROL SYSTEM PARAMETERS

Parameters		Value
Symbol	**Description**	
DG Inverter, Output Filter and Line Impedance		
V_{dc}/ V_{MG}	DC voltage/ MG voltage	650/ 311 V
f/ f_s	MG frequency/ Switching frequency	50/ 10k Hz
$P_{max\_1/2/3}$	Maxiumum output power of DG 1/2/3	1 kW
L_f/ C_f	Filter inductance/ Filter capacitance	1.8 mH/ 25 μF
Loads		
R_{load1}/ R_{load2}	Common load #1/ Common load #2	230/ 230 Ω
Primary control Loops		
k_{pi}	Proportional term in current controller	0.07
K_{ii}	Integral term in current controller	0
K_{pv}	Proportional term in voltage controller	0.04
K_{iv}	Integral term in voltage controller	94
K_{p_PLL}	PLL proportional term	1.4
K_{i_PLL}	PLL integral coefficient	1000

20, and 30 Wh, respectively. Fourth, the maximum output power of each DG unit was assumed to be 1000 W.

A. Experimental results with conventional power-sharing control

The experimental results of SoC values, output powers, and SoC change rates for DGs using the traditional power sharing control strategy are illustrated in Figs. 6 (a), (b), and (c), respectively. The figures show that the three DG units were operating on a parallel level at the beginning, with equal output powers feeding about 209 W by means of the proposed primary control with the same virtual resistances to supply the common load #1. In this condition, their SoC values decreased at different rates because the rated capacities of the ESSs were different. At 50 s, an extra 230 Ω load was connected to the parallel-connected DG system, which caused an approximated 209 W of real power step change in each DG unit. With the unified output power, SoC_1 decreased fastest because of the smallest ESS capacity of DG #1. At 87s, DG #1 was shut down as SoC_1 reached 0.3, as shown in Fig. 6 (a). Meanwhile, the real power outputs of DG #2 and DG #3 increased by 200 W, respectively, to supply the needed load, which intensely decreased the SoC_2 and SoC_3, as shown in Figs.6 (a) and (b).

At 129 s, DG #2 was suddenly shut down as SoC_2 reached 0.3, leaving DG #3 to solely supply the total amount of needed power. As displayed in Fig. 6 (b), the output power of DG #3 had to increase to 1160 W, which is over the maximum output

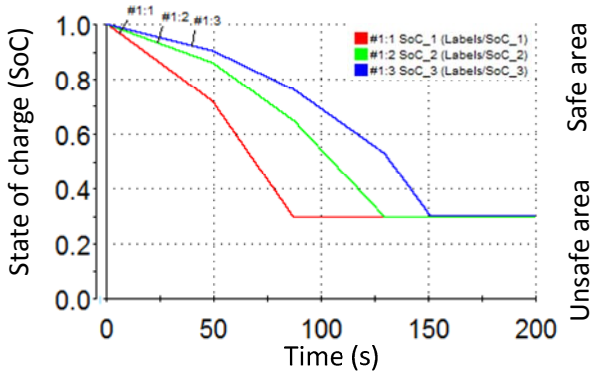

(a) SoC of ESSs.

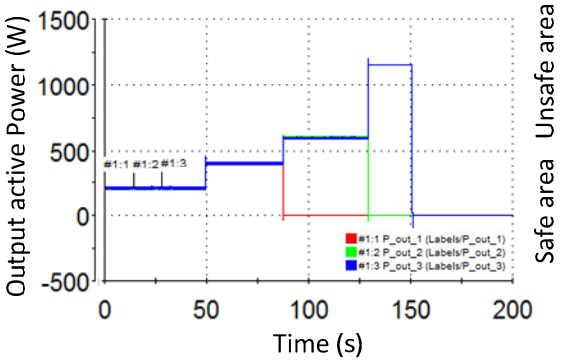

(b) Active power outputs of DGs.

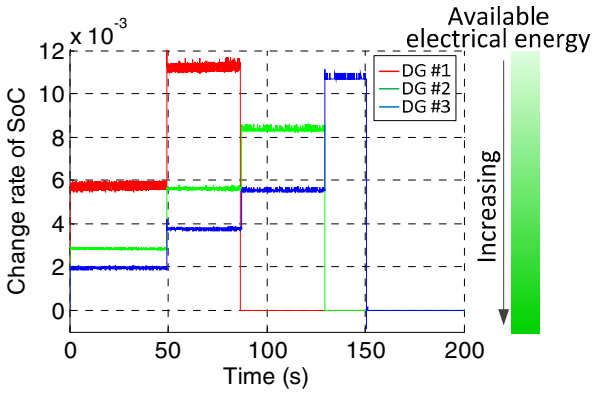

(c) Change rates of SoC.

Fig. 6. Experimental results with the conventional power sharing control.

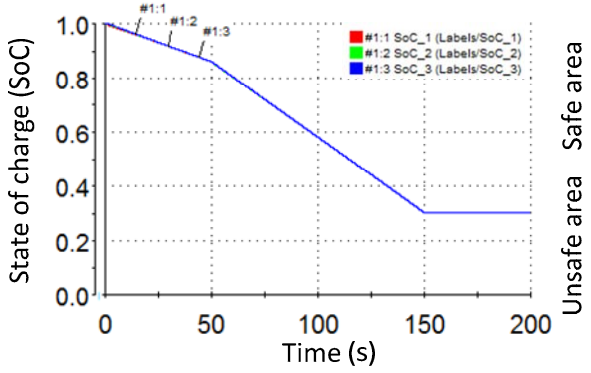

(a) SoC of ESSs.

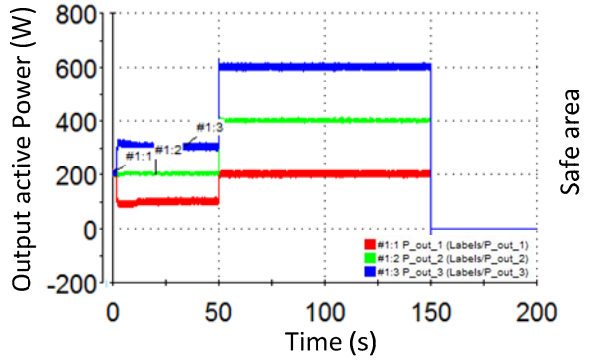

(b) Active power output of DGs.

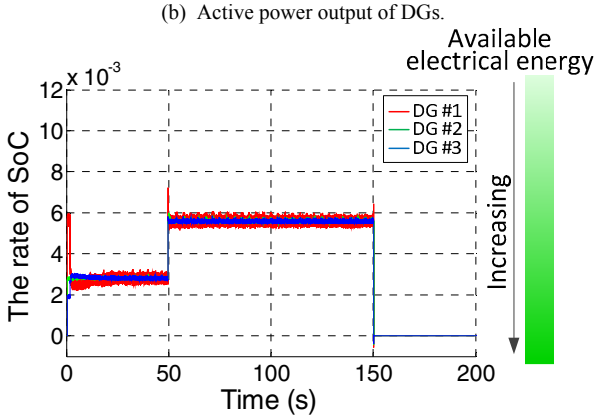

(c) Change rate of SoC.

Fig. 7. Experimental results with the proposed dynamic consensus algorithm-based coordinated control.

power of each DG (P_{max_3}). Obviously, there is a serious risk resulting in operation failure because of over current in real application. In this condition, the rated capacities of all the DGs have to be increased for allowance in order to avoid affecting MG reliability. Moreover, in practice, the faster the ESSs discharge, the less the electrical energy can be obtained.

B. Experimental results with proposed dynamic consensus algorithm-based coordinated control strategy

The experimental results of SoC values, output powers, and SoC change rates for DGs with the proposed dynamic consensus algorithm-based coordinated control strategy are illustrated in Figs. 7 (a), (b), and (c), respectively. In this test, the virtual resistance of each DG unit was regulated based on the difference between the measured SoC and SoC reference output from the distributed dynamic consensus-based coordinated controller. The SoC reference output was related to different ESS capacities. As mentioned, each DG unit only communicates its SoC state to adjacent DGs when obtaining a new SoC state via linear equation. Finally, the adaptive virtual resistance ratio will determine the power-sharing ratio among the connected DG units. Fig. 7 (a) shows that, at the beginning, three DG units were operating in a parallel manner without any coordinated control. After approximately 5 s, the proposed coordinated secondary controller starts to act. Then, the SoC values decrease with the same gradient from the original. While, since the ESS capacities of these three DG units were pre-assigned at 10/20/30 Wh (a ratio of 1:2:3), the load-power sharing ratio among the parallel-connected DG units was alsoequal to 1:2:3. At 50 s, the output powers of DG units were

increased in proportion to the 1:2:3 because of the load step-up change. At 150 s, SoC_1, SoC_2, and SoC_3 decreased to 0.3 simultaneously. This control performance is guaranteed by means of the proposed coordinated secondary controller and the adaptive VRs in primary level. Notably, overcurrent never appeared during this test, which means that operation failure can be effectively prevented. Therefore, the reliability of the entire system can be improved. Additionally, the redundant capacities and costs of the DG units can be reduced. Furthermore, the lower discharge rate of ESS by means of the proposed coordinated controller, as shown in Fig. 7 (c), can help ESSs to provide more electrical energy.

VI. Conclusions

A dynamic consensus algorithm-based coordinated secondary control with a novel autonomous current sharing control strategy for balanced discharge rate of ESSs in islanded AC MGs was proposed in this paper. Compared to previously proposed methods, this approach can not only ensure balanced discharge rate among DGs to provide higher reliability, expandability, and flexibility, but also achieves various improvements, such as achieving faster response, more accurate output current sharing, and larger stability margin. Root locus in the *z*-domain from a discrete state-space model with the proposed SoC coordinated controller shows the low sensitivity of the parameters of the proposed controller over the system dynamics. Finally, experimental results during the communication fault verify the effectiveness and flexibility of the proposed controller.

References

[1] J. Guerrero, L. de Vicuna, J. Matas, M. Castilla, and J. Miret, "A wireless controller to enhance dynamic performance of parallel inverters in distributed generation system," *IEEE Trans. Power Electron.*, vol. 19, no. 5, pp. 1205–1213, Sep. 2004.

[2] K. Jong-Yul, J. Jin-Hong, K. Seul-Ki, C. Changhee, P. June-Ho, K. Hak-Man, and N. Kee-Young, "Cooperative control strategy of energy storage system and microsources for stabilizing the microgrid during islanded operation," *IEEE Trans. Power Electron*., vol. 25, no. 12, pp. 3037–3048, Dec. 2010.

[3] H. Bode, *Lead Acid Batteries*. New York: Wiley, 1977.

[4] G. L. Soloveichik, "Battery technologies for large-scale stationary energy storage," *Annu. Rev. Chem. Biomol. Eng.*, vol. 2, no. 1, pp. 503–527, 2011.

[5] Y.-K. Chen, Y.-C. Wu, C.-C. Song, and Y.-S. Chen, "Design and implementation of energy management system with fuzzy control for DC microgrid systems," IEEE Trans. Power Electron., vol. 28, no. 4, pp. 1563–1570, Apr. 2013.

[6] Guerrero, J.M., Chandorkar, M., Lee, T., Loh, P.C., "Advanced Control Architectures for Intelligent Microgrids—Part I: Decentralized and Hierarchical Control," *Industrial Electronics, IEEE Transactions on*, vol.60, no.4, pp.1254-1262, April 2013.

[7] Y. Guan, J. M. Guerrero, J. C. Vasquez. "Coordinated secondary control for balanced discharge rate of energy storage system in islanded microgrids," *Power Electronics and ECCE Asia (ICPE-ECCE Asia), 2015 International Conference on*, 1-5 June 2015, Seoul, PP: 475 – 481.

[8] Xiaonan Lu, Kai Sun, Guerrero, J.M.; Vasquez, J.C.; Lipei Huang, "State-of-Charge Balance Using Adaptive Droop Control for Distributed Energy Storage Systems in DC Microgrid Applications," *Industrial Electronics, IEEE Transactions on*, vol.61, no.6, pp.2804,2815, June 2014

[9] T. Dragicevic, J. Guerrero, J. Vasquez, and D. Skrlec, "Supervisory control of an adaptive-droop regulated DC microgrid with battery management capability," *IEEE Trans. Power Electron*., vol. 29, no. 2, pp. 695–706, Feb. 2013.

[10] Kakigano, H.; Miura, Y.; Ise, T., "Distribution Voltage Control for DC Microgrids Using Fuzzy Control and Gain-Scheduling Technique," *Power Electronics, IEEE Transactions on*, vol.28, no.5, pp.2246-2258, May 2013.

[11] Chendan Li, Dragicevic, T., Diaz, N.L., Vasquez, J.C., Guerrero, J.M., "Voltage scheduling droop control for State-of-Charge balance of distributed energy storage in DC microgrids," *Energy Conference (ENERGYCON), 2014 IEEE International*, 13-16 May 2014, Cavtat, pp: 1310-1314.

[12] Chendan Li, Garcia Plaza, M., Andrade, F., Vasquez, J.C., Guerrero, J.M., "Multiagent based distributed control for state-of-charge balance of distributed energy storage in DC microgrids," *Industrial Electronics Society, IECON 2014*, Oct. 29 2014-Nov. 1 2014, Dallas, pp: 2180 – 2184.

[13] N. L. Diaz, T. Dragicevic, J. C. Vasquez, J. M. Guerrero. "Fuzzy-logic-based gain-scheduling control for state-of-charge balance of distributed energy storage systems for DC microgrids," *Applied Power Electronics Conference and Exposition (APEC), 2014 Annual IEEE*, 16-20 Mar. 2014, Fort Worth, TX, pp: 2171 - 2176.

[14] Diaz, N.L., Dragicevic, T., Vasquez, J.C., Guerrero, J.M. "Intelligent Distributed Generation and Storage Units for DC Microgrids—A New Concept on Cooperative Control Without Communications Beyond Droop Control," *Smart Grid, IEEE Transactions on*, vol. 5, no. 5, pp: 2476 – 2485, Sept. 2014.

[15] R. Olfati-Saber, J. A. Fax, and R. M. Murray, "Consensus and cooperation in networked multi-agent systems," *Proceedings of the IEEE*, vol. 95, no. 1, pp. 215–233, Jan. 2007.

[16] D. Spanos, R. Olfati-Saber, and R. Murray, "Dynamic consensus for mobile networks," *in IFAC World Congress*, 2005.

[17] Yasser A. I. Mohamed, Ehab F. El-Saadany. "Adaptive Decentralized Droop Controller to Preserve Power Sharing Stability of Paralleled Inverters in Distributed Generation Microgrids," *IEEE Transactions on Power Electronics*, vol. 23, no. 6, pp.2806-2816, Nov. 2008

[18] Yajuan Guan, Vasquez, J.C., Guerrero, J.M., Alves Coelho, E.A. "Small-signal modeling, analysis and testing of parallel three-phase-inverters with a novel autonomous current sharing controller," *Applied Power Electr. Conf. and Expo. (APEC)*, 2015 IEEE, pp. 571 – 578, Charlotte, NC, 15-19 Mar. 2015.

[19] N. Pogaku, M. Prodanovic, and T. C. Green, "Modeling, analysis and testing of autonomous operation of an inverter-based microgrid," *IEEE Trans. Power Electron*., vol. 22, no. 2, pp. 613–625, Mar. 2007.

[20] Meng, L., Dragicevic, T., Roldan-Perez, J., Vasquez, J.C., Guerrero, J.M., "Modeling and Sensitivity Study of Consensus Algorithm-Based Distributed Hierarchical Control for DC Microgrids," *Smart Grid, IEEE Transactions on*, vol., no.99, pp., May. 2015.

[21] Guan, Y., Guerrero, J.M., Zhao, X., Vasquez, J.C., Guo, X. "A New Way of Controlling Parallel-Connected Inverters by Using Synchronous-Reference-Frame Virtual Impedance Loop—Part I: Control Principle," *Power Electronics, IEEE Transactions on*, vol. 31, no. 6, pp: 4576 - 4593, June. 2016.

[22] Bhangu, B.S.; Bentley, P.; Stone, D.A.; Bingham, C.M., "Nonlinear observers for predicting state-of-charge and state-of-health of lead-acid batteries for hybrid-electric vehicles," *Vehicular Technology, IEEE Transactions on* , vol.54, no.3, pp.783,794, May 2005

[23] L. Xiao and S. Boyd, "Fast linear iterations for distributed averaging," *in Proc. 42nd IEEE Int. Conf. Decis. Control*, vol. 5. Maui, HI, USA, 2003, pp. 4997–5002.

[24] A. Kaveh. Optimal Analysis of Structures by Concepts of Symmetry and Regularity, *Springer-Verlag Wien*, 2013.